PERGAMON

Journal of Atmospheric and Solar-Terrestrial Physics 64 (2002) 1337–1349

Journal of ATMOSPHERIC AND SOLAR-TERRESTRIAL PHYSICS

www.elsevier.com/locate/jastp

Modeling the low-latitude thermosphere and ionosphere

C.G. Fesen[a,*], D.L. Hysell[b], J.M. Meriwether[b], M. Mendillo[c], B.G. Fejer[d], R.G. Roble[e], B.W. Reinisch[f], M.A. Biondi[g]

[a] *Center for Space Sciences, The University of Texas at Dallas, Richardson, TX 75083, USA*
[b] *Department of Physics and Astronomy, Clemson University, Clemson, SC 29634-1911, USA*
[c] *Center for Space Physics, Boston University, Boston, MA 02215, USA*
[d] *Center for Atmospheric and Space Science, Utah State University, Logan, UT 84322-4405, USA*
[e] *High Altitude Observatory, National Center for Atmospheric Research, Boulder, CO 80307-3000, USA*
[f] *Center for Atmospheric Research, University of Massachusetts at Lowell, Lowell, MA 01854, USA*
[g] *Department of Physics and Astronomy, University of Pittsburgh, Pittsburgh, PA 15260, USA*

Abstract

The National Center for Atmospheric Research thermosphere/ionosphere/electrodynamic general circulation model (TIEGCM) is one of the few models that self-consistently solves the coupled equations for the neutral atmosphere and ionosphere. Timely questions are how well the TIEGCM currently simulates the low-latitude ionosphere and what modifications might bring about better predictions. Comparisons between data obtained in and around Jicamarca, Peru, near the magnetic equator, and simulations with the TIEGCM indicate good progress has been made but reveal some serious discrepancies. Good-to-excellent agreement is obtained for electron densities, electron and ion temperatures, and n_{max}. The agreement is fair to poor for h_{max}, zonal drifts, the 630 nm oxygen nightglow, and the horizontal neutral winds. The most important discrepancy is in the simulated neutral temperature, which is at least 100 K too cold relative to Fabry–Perot interferometer observations. Increasing the EUV fluxes in the model to improve prediction of the model temperature also improves representation of airglow observations and of the ionosphere, for which the model typically underrepresents the electron densities. The disparity in neutral temperature is also present in comparisons with the empirical model MSIS which represents the largest database of thermospheric temperature measurements. Since the neutral and ionized atmospheres are tightly coupled at low latitudes, simultaneous measurements of neutral and ion parameters, preferably over an extended time period, would be invaluable to further the understanding of the region. Better knowledge of the EUV fluxes and the high altitude O^+ fluxes may also help resolve some of the model/data discrepancies.

Keywords: Modeling; Thermosphere dynamics; Ionosphere dynamics; Low latitudes; Electron densities

1. Introduction

Two thermospheric general circulation models are currently capable of self-consistently simulating the coupled thermosphere/ionosphere system: the National Center for Atmospheric Research (NCAR) thermosphere/ionosphere/electrodynamic general circulation model (TIEGCM) (e.g., Richmond et al., 1992) and the coupled thermosphere/ionosphere/plasmasphere (CTIP) model (e.g., Fuller-Rowell et al., 1996; Millward et al., 1996) developed at University College-London and the National Oceanic and Atmospheric Administration Space Environment Center.

Both models recently achieved a breakthrough in that they now simulate the pre-reversal enhancement (PRE) in the low-latitude vertical ion drifts. The TIEGCM reproduces the full seasonal and solar cycle variation of the F region vertical and zonal ion drifts (Fesen et al., 2000). Before the models are used to investigate physical processes such as the mechanism for producing the PRE, it is necessary to ascertain how realistically they simulate the atmosphere and

* Corresponding author. Tel.: +1-972-883-2815; fax: +1-972-883-2761.
E-mail address: fesen@tides.utdallas.edu (C.G. Fesen).

1364-6826/02/$ - see front matter
PII: S1364-6826(02)00098-6

ionosphere. The low-latitude ionosphere, in particular, is a region that has been relatively little investigated with the TIEGCM. Coincidentally, observations of this region have been accumulating over the last few years, particularly from the National Science Foundation's (NSF) Coupling, Energetics, and Dynamics of Atmospheric Regions (CEDAR) initiative MISETA (Multi-Instrumented Studies of Equatorial Aeronomy). It is therefore timely to consider the question of how well the TIEGCM currently simulates low latitudes and what modifications might bring about better predictions.

2. Model description

The NCAR TIEGCM (Richmond et al., 1992, and references therein) self-consistently calculates electric potential, fields, and currents along with the ion and neutral densities, temperatures, and velocities. The vertical coordinate is log pressure with 29 levels spaced at 2 grid points per scale height; the altitudes extend roughly from 100 to $\geqslant 400$ km; the top altitude depends on the level of solar activity. Latitude and longitude resolution are both 5°. The model contains a realistic geomagnetic field.

An important feature of the model is the formulation of the lower boundary condition which can be used to simulate the effects of a variety of waves generated in the lower atmosphere which penetrate into the thermosphere. The model includes the diurnal 1,1 mode and the semidiurnal 2,2; 2,3; 2,4; 2,5; and 2,6 modes (e.g., Fesen et al., 1991; Forbes et al., 1993) which are adjustable parameters. Here, we adjusted the lower boundary tidal forcing to reproduce winds observed near 100 km by the Upper Atmosphere Research Satellite (e.g., McLandress et al., 1996).

Most of the simulations reported here represent geomagnetically quiet conditions for low solar activity. Specifically, the total hemispheric power of precipitating auroral electrons was 16 gW, the cross-polar-cap potential was 45 kV, and the solar 10.7-cm radiation index F10.7 was 75. The model had been previously tuned against empirical models to reproduce their global and zonal means. For the neutral atmosphere, the empirical model was the Mass Spectrometer and Incoherent Scatter radar data (MSIS) model (Hedin, 1991); the International Reference Ionosphere (IRI) (e.g., Bilitza, 1986) was used for the ionosphere. The tuning consisted of adjusting the Joule heating in the model (e.g., Codrescu et al., 1995) and the O^{+} fluxes at the model upper boundary. To reproduce the IRI predictions, it was necessary to impose downward O^{+} fluxes at the TIEGCM top boundary at all times; this point will be discussed later in the paper. The tuning of the TIEGCM global and zonal means to the empirical models helps ensure a realistic background atmosphere and ionosphere in the TIEGCM.

Three sets of model simulations are the basis of the study presented here, all of which were for October with an F10.7 index of 75: the "standard" simulation, with standard model inputs, included the semidiurnal tidal forcing at October consistent with model predictions by Forbes and Vial (1989); a "big tide" case, which increased the 2,2 amplitude at the model lower boundary by a factor of 10; and an "increased EUV" case, which increased the EUV energy input into the model by 30%, consistent with observations of the EUV variability (e.g., Schmidtke et al., 1993). The "big tide" case represents a numerical experiment to evaluate the effects of large tides on the simulated fields; underestimation of the semidiurnal tide is a long-standing problem for numerical models (e.g., Salah et al., 1991).

The data sets used for comparison are from the NSF/CEDAR initiative MISETA (http://www.dartmouth.edu/~cfesen/miseta) which fields a variety of instruments in and around the Jicamarca Radio Observatory (11.95°S, 76.87°W), Peru, near the geomagnetic equator. These observations are particularly useful for model/data comparisons because the instruments measured both the neutral and ionized atmosphere. A number of campaigns have been conducted; in particular, observations have been obtained in October for several years beginning in 1996, near solar cycle minimum. The instruments include the incoherent scatter radar (ISR) (e.g., Farley, 1991), a digisonde (e.g., Reinisch and Huang, 1999) a Fabry–Perot interferometer (FPI) (e.g., Biondi et al., 1999), and an imager from Boston University (BU) (e.g., Mendillo et al., 1997). The FPI and BU imager are located at Arequipa, Peru (16.5°S, 71.5°W).

3. Model/data comparisons

Comparisons are first made with the empirical models for a range of geophysical conditions to illustrate the TIEGCM's current capabilities. Fig. 1 shows the global mean neutral temperature, atomic oxygen mixing ratio, and electron density for March, June, and December during solar cycle minimum and maximum. In the F region, the TIEGCM neutral temperatures are within 10% of MSIS and tend to be slightly larger while the atomic oxygen mixing ratios exceed those in MSIS by a maximum of 10–20%. The largest disagreement in the global means is in the electron densities at solar maximum, when the TIEGCM underestimates the densities relative to IRI by a maximum of $\sim 50\%$ in December; at solar minimum, the differences are generally $< 20\%$.

The comparisons for the peak electron density, $n_{\max}$, and the height of the peak density, $h_{\max}$, as a function of latitude and longitude are illustrated in Fig. 2 for March solar cycle minimum and June solar cycle maximum at 00 UT. The TIEGCM tends to overestimate $n_{\max}$ at middle-to-high latitudes and underestimate $n_{\max}$ at low latitudes. For $h_{\max}$, the agreement is generally within 10 km. In terms of percentages, the TIEGCM-predicted $n_{\max}$ are usually within 50% of those in IRI. The agreement shown here is typical of that in a complete set of simulations for March, June, and December for solar cycles minimum, medium, and maximum.

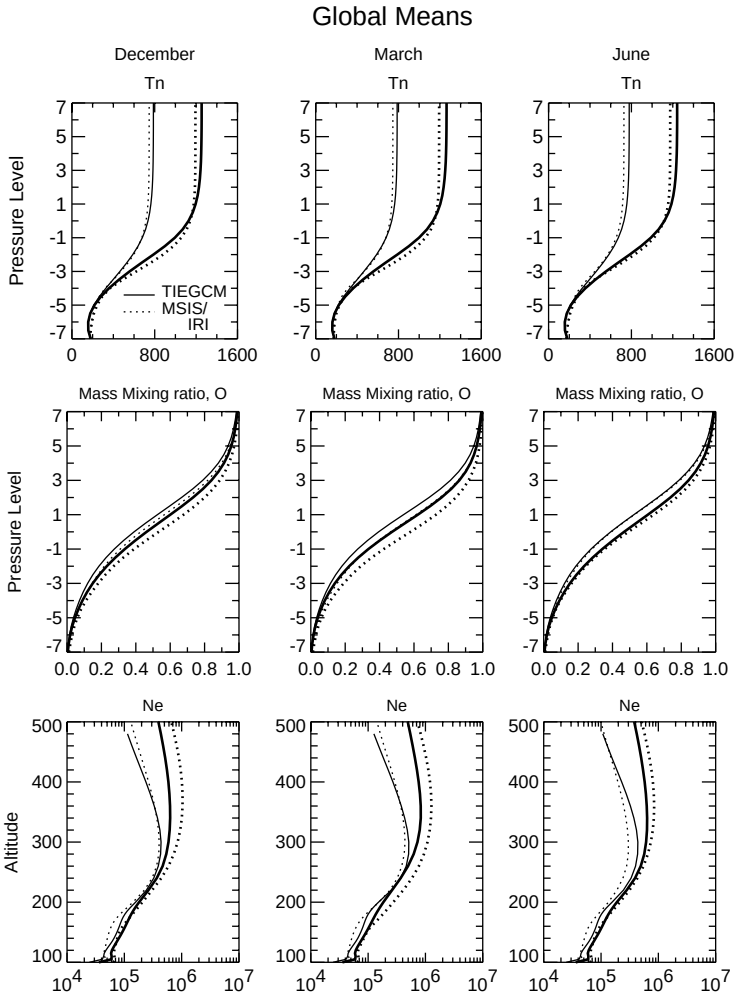

Fig. 1. Comparison of global means from TIEGCM (solid curves) and MSIS (dotted curves) for December (left column), March (middle column), and June (right column). Top row: neutral temperature; middle row: O mass mixing ratio; bottom row: electron density. Thick curves are for solar maximum, thin curves for solar minimum.

With this background, attention is now focused on model/data comparisons at low latitudes during equinox solar cycle minimum conditions, using data obtained during MISETA campaigns in October 1996 and 1997. Because of space constraints, the comparisons shown here are limited to electron densities (N_e), n_{max}, h_{max}, electron, ion, and neutral temperatures (T_e, T_i, and T_n, respectively), and the 630 nm oxygen airglow. Comparisons were also made for the horizontal neutral winds and the zonal and vertical ion drifts but are not shown here.

The neutral temperature is arguably the most fundamental parameter describing the upper atmosphere. The model/data comparison for October 1996 at Arequipa is shown in Fig. 3a. Observations from the FPI represent conditions near 260 km; crosses represent datapoints for 1996 and diamonds for 1997. Below the F peak, T_i generally approximates T_n; therefore, ISR measurements of T_i are also plotted in the figure. These data were obtained on October 10 for an altitude of 266 km. The thick solid curves show predictions from MSIS, with the higher curve resulting from increasing the F10.7 index in MSIS from 75 to 110. The thinner curves show the TIEGCM results: the thin solid curve shows "standard" calculations for October solar cycle minimum; the dotted curve shows results for the "big tide" case, and the dashed curve shows results for the "increased EUV" case. Not surprisingly, the two models agree very well with each other, since TIEGCM has been tuned to the MSIS model, but neither agrees well with the data. Both models seriously underestimate the neutral temperature near local midnight. The ISR T_i measurements better approximate the model predictions but it is likely that the observed T_i are underestimated because of the neglect of electron coulomb

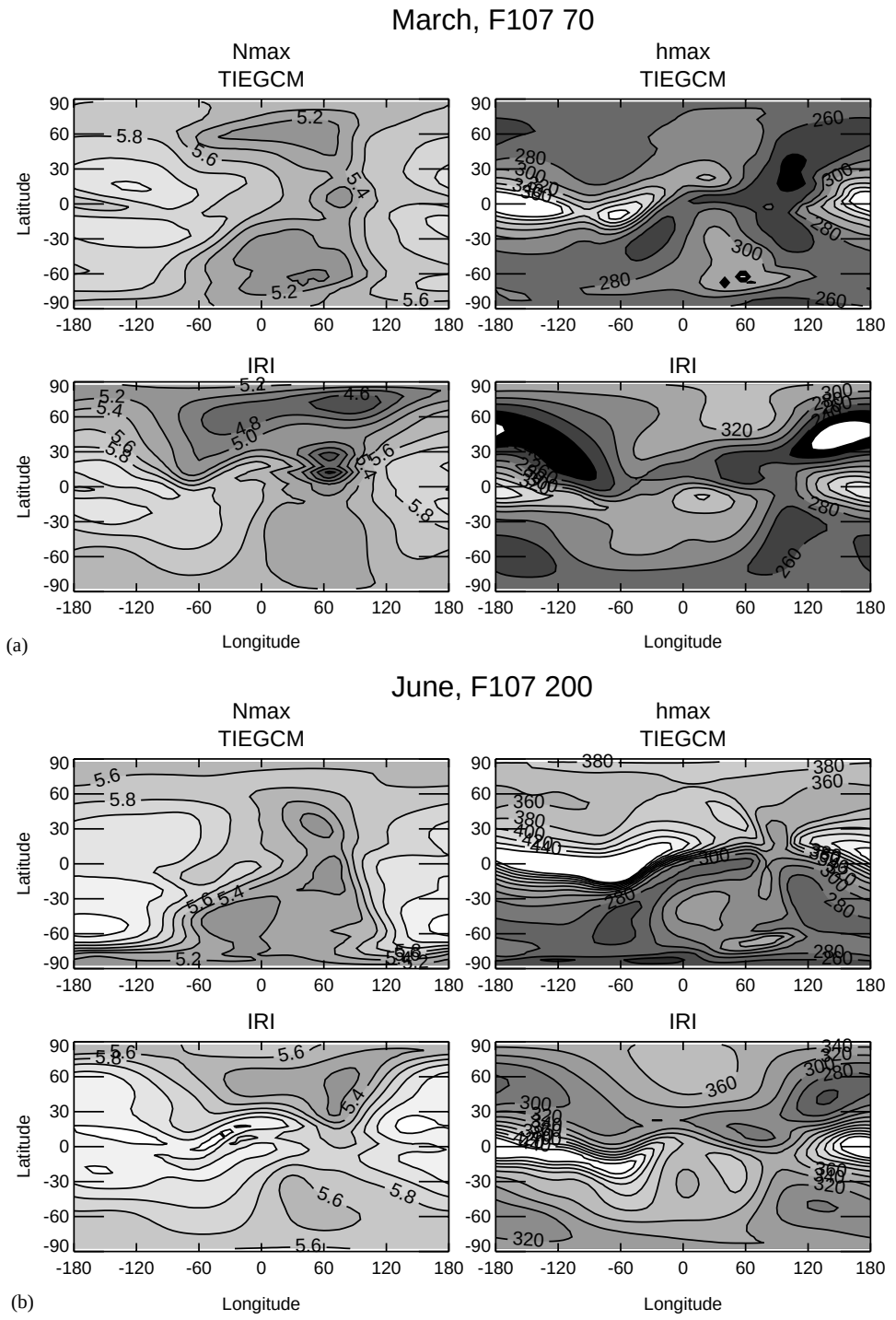

Fig. 2. Comparison of N_{max} (right) and h_{max} (left) for TIEGCM and IRI. (a). Equinox solar minimum; (b) June solar maximum.

collisions (Sulzer and Gonzalez, 1999) in the data analysis. The data also show a midnight temperature maximum (MTM) while the two models only produce a very small feature.

Hernandez and Roble (1977) reported a similar finding: neutral temperatures derived from airglow observations at Fritz Peak, Colorado, a midlatitude site, were about 150 K hotter than predicted by MSIS for equinox solar cycle

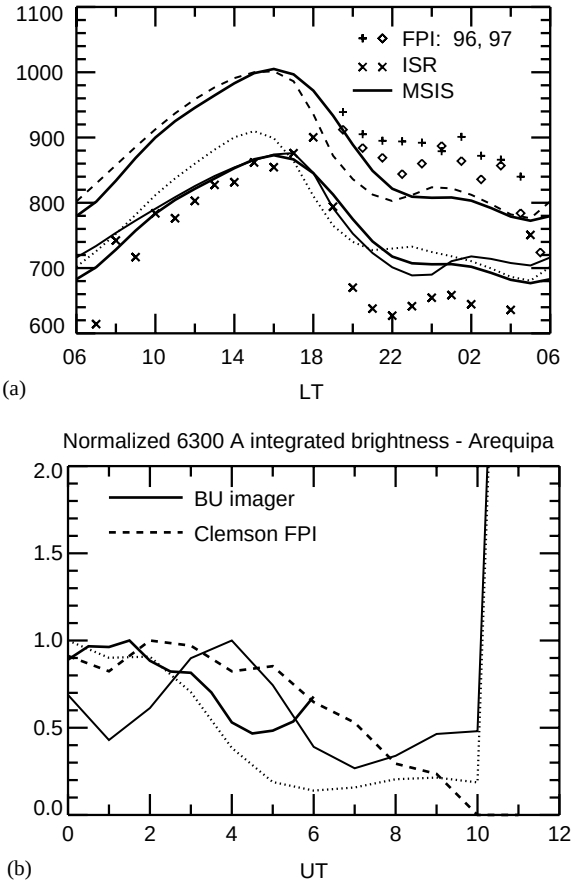

Fig. 3. (a) Comparison of neutral and ion temperatures near 260 km. Neutral temperatures from the FPI are shown by crosses for 1996, diamonds for 1997. Ion temperatures from the ISR are shown by x's Thick curves represent MSIS predictions of T_n. Thin curves represent TIEGCM predictions of T_n: solid, standard run; dotted: big tide; dashed, enhanced EUV. See text for details. (b) Normalized 630 nm integrated brightness at Arequipa. Thick curves: observations; thin curves, TIEGCM runs: solid, standard; broken, enhanced EUV.

minimum. Analysis of 14 World Day campaigns carried out by the ISR at Arecibo indicated that the radar measurements of exospheric temperature were generally about 50 K less than those predicted by MSIS for similar conditions for all local times (Burnside et al., 1991). However, in September 1986, i.e., for equinox solar cycle minimum, the radar-derived temperatures were about 50 K hotter than those predicted by MSIS, while in September 1987, also equinox solar cycle minimum, the data and MSIS model temperatures were essentially the same. Clearly, the discrepancy between temperature measurements and the model predictions is an outstanding problem.

The large observed neutral temperature (relative to the models) is consistent with observations of the integrated brightness of the 630 nm oxygen airglow measured independently by the BU imager and by the FPI which are shown in Fig. 3b. These airglow measurements provide an extremely sensitive test for magnitudes of neutral and plasma densities, reaction rates, and transport effects, with high signal-to-noise ratios on the bottomside of the F region. The BU imager data represent an average over 15 nights in October 1996 and the FPI data over 13 nights. The airglow measurements are indicated by the thick curves and are in reasonable agreement given the uncertainties in their absolute calibration. The thin curves show the TIEGCM predictions: the thin solid curve is the standard October solar minimum simulation; the dotted curve shows the results with enhanced EUV which gives a better representation of the data although it decreases too rapidly with time.

For the ionosphere, the fundamental comparison is for n_{max} and h_{max}. Observations from the ISR and the digisonde for October 1996 are shown in Fig. 4, along with the model results. Predictions from IRI are shown by the thick solid curve, from the digisonde by the thick broken curve, from the ISR by the crosses, and from the TIEGCM by the thin curves. Although the ability of the IRI to represent the low-latitude ionosphere is sometimes questioned, Abdu et al. (1998) and Szuszczewicz et al. (1990) found that IRI generally provided very good representation of n_{max} in the equatorial region when compared with global datasets obtained during SUNDIAL campaigns (e.g., Szuszczewicz et al., 1988); comparisons of h_{max} were less satisfying although still reasonable. Of particular interest for this paper is that SUNDIAL included campaigns for October solar cycle minimum, the geophysical conditions of interest here, and for these campaigns IRI and the measurements were found to be in reasonable agreement. Turning to results shown in Fig. 4, in the daytime, the TIEGCM n_{max} are smaller than those predicted by IRI and measured by the digisonde and ISR by up to 40%; the agreement with IRI and the digisonde tends to be better from 22 to 06 LT. Before 18 LT, the enhanced EUV simulation best agrees with the datasets; after 22 LT, the standard run is a better representation of the IRI and observed densities. For h_{max}, there are discrepancies between the two instruments, between the two models, and between the data and the models. The two models generally predict higher h_{max} than the instruments to about 20 LT, with TIEGCM predicting the largest heights. After 22 LT, there are significant differences among all the curves for h_{max}.

Sample altitude profiles are shown in Fig. 5 for N_e, T_e, and T_i. Profiles are shown at 03, 09, 15, and 21 LT to illustrate the variety of possible results. The IRI and TIEGCM simulations are shown by the thick curves. Note that above the F peak, the digisonde measurements are fit to a Chapman profile and this extrapolation is what is plotted in the figure. The ISR measurements are shown by crosses. The diamonds show digisonde measurements of N_e made on the same day as the ISR measurements; digisonde data were not available at all local times. The monthly mean of the digisonde observations for October 1996 is indicated by the dot–dash curve. Note

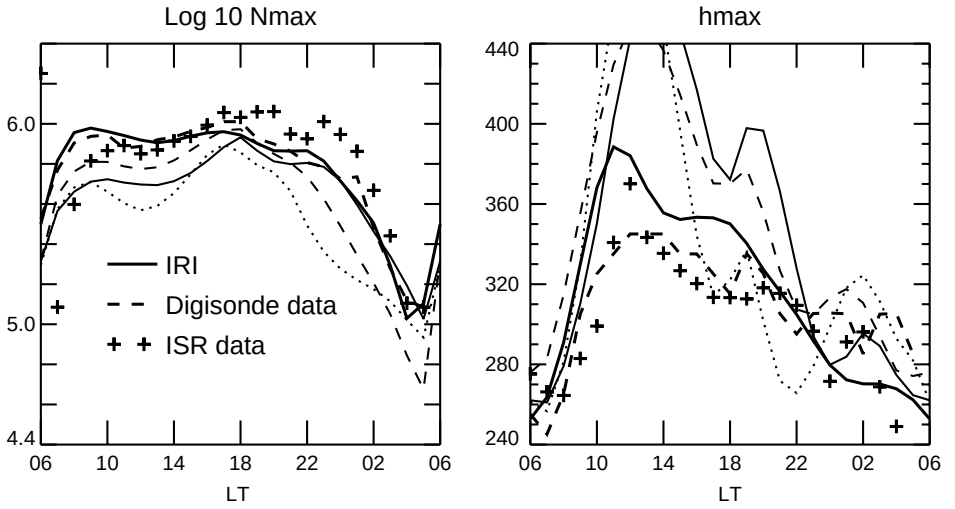

Fig. 4. Comparisons of N_{max} and h_{max} at Jicamarca. Thick curve, IRI; broken curve, digisonde data; crosses, ISR measurements. Thin curves, TIEGCM: solid: standard; dotted, big tide; dashed, enhanced EUV.

that at night, the algorithms for ISR data analysis assume that $T_e = T_i$; further, the effect of electron coulomb collisions are ignored which results in possible underestimation of T_e (Sulzer and Gonzalez, 1999). The TIEGCM and IRI often agree with each other very well (e.g., at 03 LT for N_e and T_i) but not necessarily with the datasets which can also exhibit discrepancies: at 03 LT, for N_e, the digisonde daily observations and those from the ISR differ by an order of magnitude. This panel also shows that the digisonde-derived monthly mean N_e can differ substantially from data on a particular day. For N_e, in general, TIEGCM tends to predict smaller densities than IRI; above 200 km, the agreement is generally better than a factor of two.

Comparisons for T_e and T_i are shown in Figs. 5b and 5c, respectively. For T_e, TIEGCM and IRI typically agree within 20%; largest discrepancies occur near the location of the daytime peak which tends to occur at higher altitudes in IRI and is narrower than in TIEGCM. Both models appear to overestimate the T_e observations in general but, as mentioned earlier, these may be too small. For T_i, the agreement between IRI and TIEGCM is generally within 60 K or 10%. This is because TIEGCM has been tuned to MSIS, and MSIS is used in IRI to simulate the neutral temperatures which are identical to T_i during nighttime. However, there can be substantial disagreement with observations, e.g., at 03 LT.

As mentioned earlier, comparisons were also made for other parameters but space constraints preclude presenting the relevant figures here. The model/data agreement can be qualitatively described as follows:

Good to excellent agreement is found for N_e, T_e, T_i, vertical drifts, and n_{max}. The model vertical drifts strongly depend on the semidiurnal tides. For n_{max}, the model/data agreement improves if larger EUV fluxes are used in the model.

Fair-to-good agreement is found for h_{max}, the zonal winds and drifts, and the 630 nm airglow. In the model, the daytime zonal drifts are very sensitive to the tidal input at the lower boundary.

Poor agreement is found for T_n and the meridional winds. In particular, the neutral temperatures in both MSIS and TIEGCM are too cold by > 100 K relative to the observations.

Since the neutral composition is not measured, the model performance in this area is unknown.

The obvious question is what is needed to model the low-latitude atmosphere and ionosphere more realistically. Assuming that the physics and chemistry in the models are correct (a point discussed further later), and that the time and space scales being investigated are appropriate to the particular model, the options in self-consistent models such as the TIEGCM and the CTIP are limited to adjusting model inputs and the model boundary conditions. Specifically, the possibilities involve the (1) high-latitude forcings; (2) upper boundary conditions; and (3) lower boundary conditions. Each of these is discussed briefly below.

The high-latitude forcings are the energy and momentum inputs associated with the Joule heating and magnetospheric convection that occur in and near the auroral oval. In the TIEGCM, the relevant parameterizations are the hemispheric power and the cross-polar-cap potential which are used to define the location and half-width of the auroral oval and the amount of energy being deposited into it. The standard inputs to the model for these two parameters occur in pairs and are listed in Table 1, along with a rough estimate of the corresponding K_p level. However, such a parameterization neglects much of the small-scale structure at high latitudes, particularly in the electric field, which can

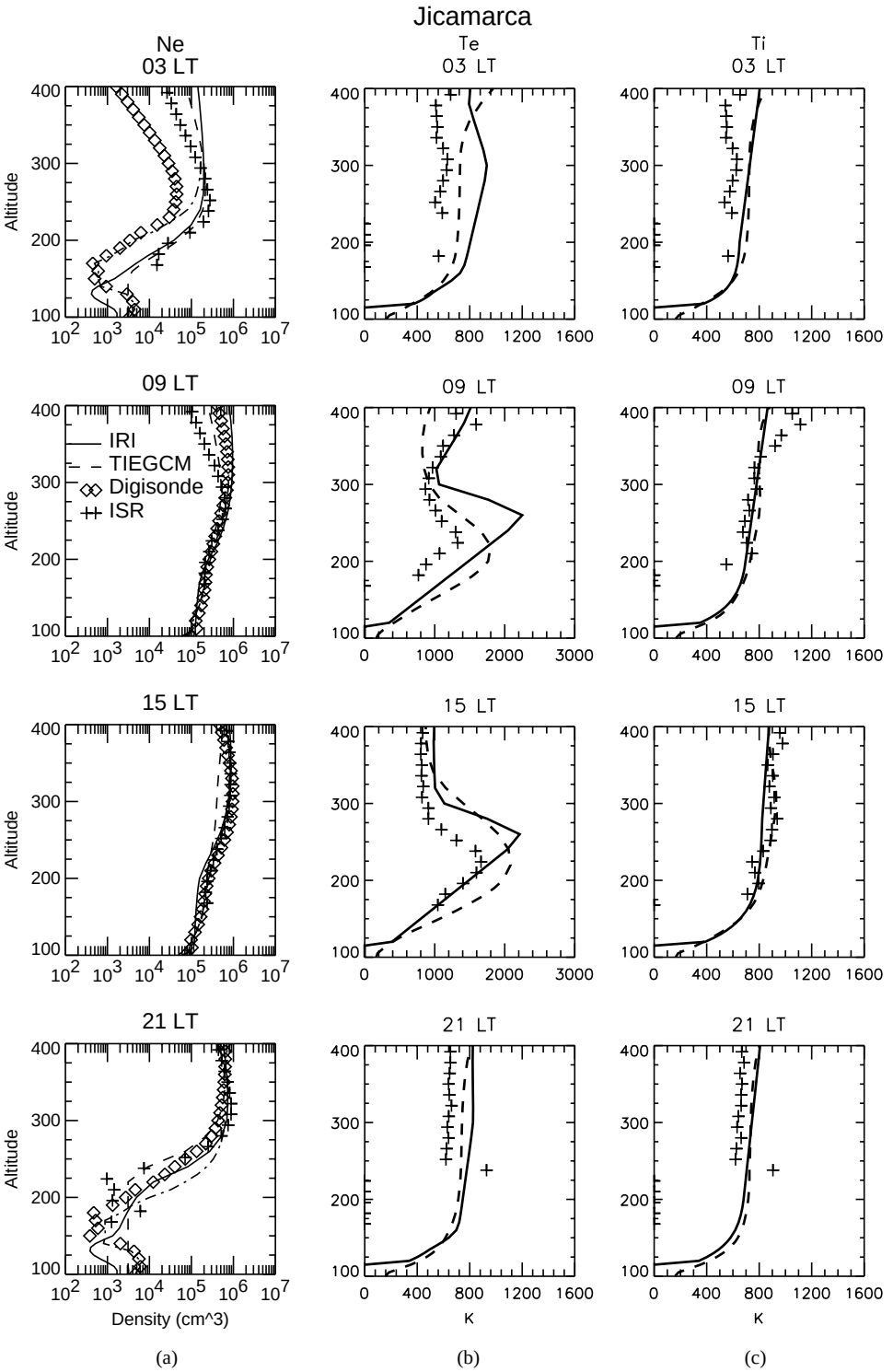

Fig. 5. Observations and model predictions for Jicamarca for October during solar cycle minimum. See text for details.

Table 1
Auroral input parameters

H. power (gW):	2	3	5	7	11	16	23	33	48	82	115
Potential (kV):	20	30	40	50	60	70	80	90	100	115	130
Rough K_p:		0	1	2	3	4	5	6			

cause ion drag and Joule heating in localized regions smaller than the grid size used in general circulation models such as the TIEGCM and CTIP which results in an underestimate of the energy and momentum inputs at high latitudes (Codrescu et al., 1995). The effect is important because, as first noted by Dickinson et al. (1975), the heating driven by the high-latitude forcings is an important element in global energy balance of the atmosphere and must be included in the thermospheric energy budget even during geomagnetically quiet conditions. The model neutral temperature and composition, in particular, are strongly dependent on the specification of the high latitudes. Codrescu et al. (1995) suggested a multiplicative factor be applied to the Joule heating in the models to account for the underestimate. By trial and error, it was determined that using inputs of 16 gW for hemispheric power and 45 kV for cross polar cap potential resulted in a global and zonal mean neutral atmosphere in good agreement with MSIS. Away from the poles, the ionized atmosphere is relatively insensitive to the representation of the auroral region. Earlier investigations by Fesen (1997) showed that changes in the high latitude forcing affected n_{max} and h_{max} at low latitudes on the order of 10%.

The effect of the upper boundary condition on the model atmosphere has been relatively little explored in the TIEGCM. One of the boundary conditions is the flux of O^+ which can have substantial impact on the ionosphere (e.g., Park and Banks, 1974). The flux is generally considered to be upward by day and downwards at night; typical values are on the order of 10^8 cm^{-3} s^{-1}. In the TIEGCM, the flux is usually specified by two numbers representing the daytime flux and the nighttime flux. Further, the flux is assumed invariant with longitude; it varies sinusoidally with geographic latitude from zero at the equator to a maximum at 60° latitude above which it is constant. It is also invariant with local time, save for distinguishing between daytime and nighttime. Here, attention is focused on just three of the test cases performed, which differed from each other only in the O^+ flux specified at the model upper boundary; the inputs for these three cases are listed in Table 2.

The resulting global mean electron density and electron and ion temperatures are shown in Fig. 6. The typical fluxes of ± 1.5–3.0×10^8 cm^{-3} s^{-1} produce a significant underestimate of N_e, which causes the model T_e to be much larger than predicted by IRI. Downward fluxes are needed to produce good agreement with the empirical IRI electron densities.

Table 2
O^+ flux at upper boundary (cm^{-3} s^{-1})

Day	Night
$+1.5 \times 10^8$	-1.5×10^8
$+3.0 \times 10^8$	-3.0×10^8
-9.0×10^8	-3.0×10^8

+ Indicates upward flux; − downward flux.

The effects of the O^+ flux on n_{max} and h_{max} at Jicamarca are indicated in Fig. 7, along with the predictions from IRI. The "standard" flux of $\pm 1.5 \times 10^8$ cm^{-3} s^{-1} results in an underestimate of both n_{max} and h_{max} in the TIEGCM; increasing both the day and night fluxes causes the agreement to deteriorate. Best agreement for n_{max} occurs using fluxes that are downward in both day and night. However, the agreement for h_{max} remains poor and is generally worst in daytime for the fluxes that are always downward.

The lower boundary of the TIEGCM includes the parameterization of propagating tidal waves including the 2,2; 2,3; 2,4; 2,5; and 2,6 semidiurnal modes and the 1,1 diurnal tide. The effect of the tides at the lower boundary on the modeled n_{max} and h_{max} was reported by Fesen (1997): changes to n_{max} and h_{max} were on the order of 10–20% during the day and up to 40% at night, depending on latitude. The various atmospheric species must also be specified at the lower boundary, either as densities or mass mixing ratios or via a flux condition but these will not be discussed here. The focus is on how the tides and the electron densities near the lower boundary affect the electrodynamics. Results are presented in Fig. 8 which shows the ion drifts near the magnetic equator, both calculated and observed, and how they respond to some test cases. The thick curves show the averaged equinox solar cycle minimum drifts as assembled by Fejer et al. (1991); the vertical drifts are typically upwards by day and downwards at night, with an enhancement in the upward drift, the PRE, before it reverses direction near sunset. The zonal drifts are generally westward by day and eastward at night with largest eastward drifts dependent on the magnitude of the PRE in the vertical ion drifts. The sensitivity study to investigate the effects of the E region electron densities on the PRE was done by varying the specification of N_e near the model lower boundary which affects the densities throughout the E region; some of the results are presented in Fig. 8a, which plots the electron densities near 125 km, near the peak of

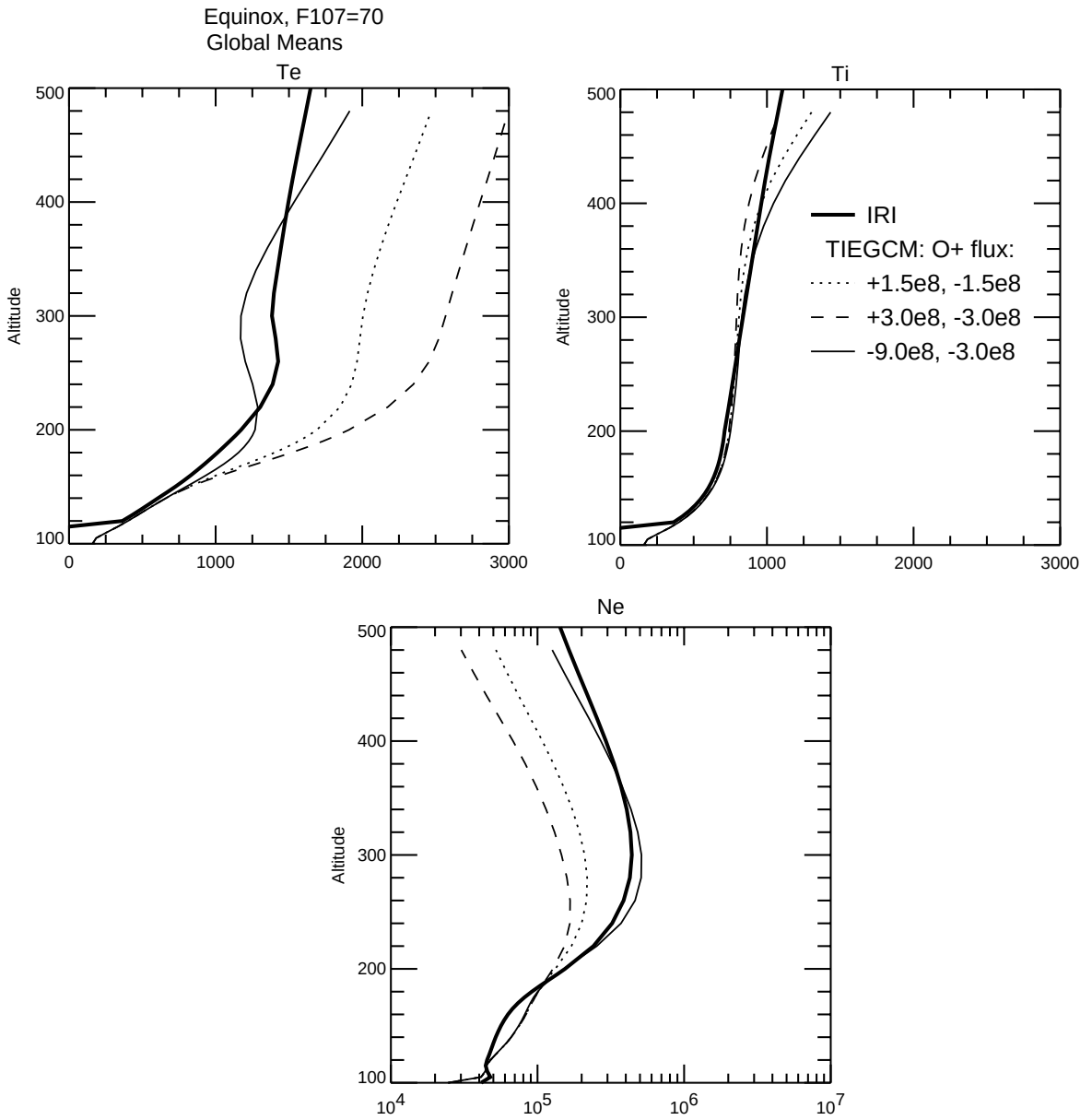

Fig. 6. TIEGCM calculations of global means for equinox, solar cycle minimum, for different O^+ fluxes at the model upper boundary. IRI predictions are shown by the thick solid curve.

the Pedersen conductivity. The figure suggests that, in the model ionosphere, the nighttime *E* region electron density determines whether the PRE develops. As the electron density decreases, the PRE becomes stronger which affects the zonal ion drifts near 20 LT, causing them to become more like the observations. The effects of altering the *E* region electron density, however, are limited to the nighttime and thus do nothing to ameliorate the underestimate of the daytime vertical drifts in the model. The model daytime drifts were found to be affected most strongly by the 2,2 semidiurnal tide, as shown in Fig. 8b. As the amplitude increases, the daytime drifts increase. It was found that increasing the 2,2 amplitude to a value roughly three times that suggested by Forbes and Vial (1989) for equinox provided the best agreement with the ISR observations, as first reported by Fesen et al. (2000). The increased 2,2 amplitude would help ameliorate the underestimate of the semidiurnal tides in the lower thermosphere that was noted in the Introduction. The slight phase difference in the time of the daytime maximum could be resolved by changing the phase of the 2,2 mode.

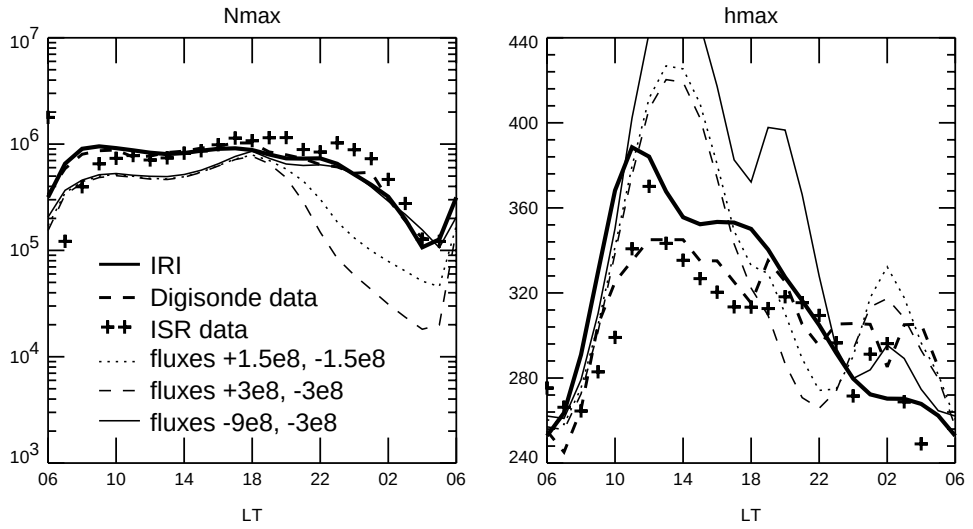

Fig. 7. N_{max} and h_{max} at Jicamarca during October solar cycle minimum. Crosses: ISR data. Thick solid curves: IRI predictions; thick broken curve: digisonde observations. Thin curves are TIEGCM simulations which varied O^+ fluxes at the model upper boundary.

Whether the observed daytime drifts can be used to infer information on the semidiurnal tides is an intriguing possibility that should be investigated further.

4. Summary and discussion

The low-latitude ionosphere has been relatively little explored in terms of large-scale self-consistent theoretical models. Comparisons between data obtained in and around Jicamarca, Peru, near the magnetic equator, and simulations with the NCAR TIEGCM indicate good progress has been made but reveal some serious discrepancies. The most important discrepancy is in the simulated neutral temperature, which is at least 100 K too cold relative to FPI observations. Interestingly, increasing the EUV fluxes in the TIEGCM to improve the prediction of the temperature also improves the representation of airglow observations and the ionosphere, for which the TIEGCM typically underrepresents the electron densities.

The discrepancy in neutral temperature is also present in comparisons with the empirical model MSIS which represents the largest database of thermospheric temperature measurements. Very few ground-based measurements at low latitudes were available for inclusion in the empirical models; much of the data for this region arises from satellites such as the Orbiting Geophysical Observatory (OGO), Dynamics Explorer (DE), Atmosphere Explorer (AE), and San Marco. If the spacecraft are polar-orbiting, as were DE and AE-C, there is limited local time coverage, and this is typically aliased with the seasonal coverage. AE-E and the San Marco satellites were equator-orbiting but AE-E measurements were largely made at solar maximum and at high altitudes while San Marco was relatively short lived. Extrapolation must be made to the conditions that are the focus of this paper: solar minimum and at lower altitudes. A separate issue is the fact that all the data in MSIS are from previous epochs of the solar cycle. The question of variability in the atmosphere and on what time scales is still very much an open question. For all these reasons, it is not clear how accurately, or indeed whether, the empirical models can represent current low-latitude atmosphere/ionosphere measurements. It is obvious that the practice of "tuning" theoretical models to empirical models, as was done here with the TIEGCM, should be further investigated.

The specification of the O^+ fluxes in the model runs presented here were downward at all times. While the plasma flows are typically expected to be upwards by day and downwards at night, these flows are generally ascribed to altitudes higher than those in the simulations here. Recall that the model upper boundary for these solar minimum conditions is only near 400–500 km, which does not represent the topside ionosphere. Evans (1975) found that the flux can change sign at some "transition" level, near 550 km; below this level, ions move downwards due to gravity. At altitudes near 300–400 km, drifts that are upwards and outwards near the equator during the day imply downward velocities at latitudes off the equator, consistent with the specification of the O^+ flux in the model runs reported here. Simulations of the O^+ flux by the field-line interhemispheric plasma model (e.g., Richards and Torr, 1988), reported by Szuszczewicz et al. (1996), suggest that the flux varies substantially with local time and latitude, unlike the parameterization used here. Since the O^+ flows can have a marked effect on n_{max} (e.g., Sica et al., 1990), and since examination of the suite of TIEGCM simulations indicates that the zonal mean n_{max} is

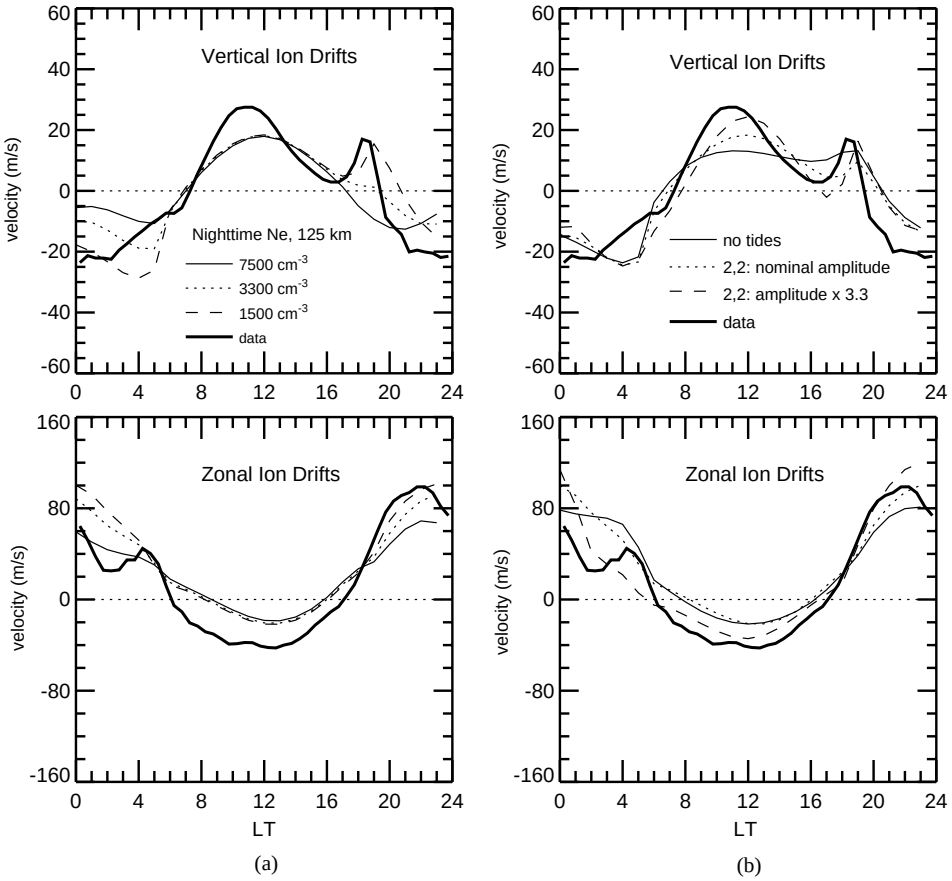

Fig. 8. Effect of varying model parameters on the observed ion drifts. Top: vertical drifts; bottom, zonal drifts: (a) varying nighttime Ne; (b) varying semidiurnal 2,2 at model lower boundary. See text for details.

typically underestimated, further sensitivity studies with the TIEGCM using more realistic O^+ fluxes appear promising to help alleviate some of the model/data discrepancies.

As noted above, at solar cycle minimum, the upper boundary of the TIEGCM is at relatively low heights (400–500 km) since the model is formulated in pressure levels, the altitudes of which vary with solar activity. The model also does not solve for H^+ densities which may be significant at high altitudes near solar cycle minimum (e.g., Burnside et al., 1988). Both these shortcomings will affect simulation of the model ionosphere and possible methods to ameliorate these shortcomings are being investigated.

Other parameters that can affect the neutral temperature and ionospheric density in the model include the O^+–O collision frequency, the EUV forcing, small-scale electric fields, and the heating efficiency of photoionization. The possible importance of small-scale electric fields at high latitudes on the global energy input was mentioned in Section 3. The O^+–O collision frequency is the dominant factor governing the energy transfer between solar radiation and the thermosphere. As noted by Oliver and Glotfelty (1996), it determines the location of h_{max} and thereby the density of the charged particles. Burnside et al. (1987) recommended a value of 1.7 times the value calculated by Banks (1966); more recent work has suggested reducing the factor to 1.25 (Pesnell, 1993); 1.15 (Buonsanto et al., 1997), and 0.75 (Oliver and Glotfelty, 1996). A value of 1.5 was used in the TIEGCM simulations reported here. Oliver and Glotfelty (1996) found that atomic oxygen densities inferred from radar measurements often exhibited episodic departures from MSIS predictions by up to 50% which could last for months. This point is important for analysis of campaign results if MSIS is used in the data reduction.

The EUV forcing in the model is typically represented by photon fluxes in a finite number of wavelength intervals. Since the fluxes vary greatly with wavelength, the solar rotation period, and the solar cycle, parameterizing the fluxes realistically is difficult. A separate issue is the relative paucity of data on the solar fluxes, particularly for the most recent solar cycle.

Once absorbed, the solar energy can heat, ionize, or dissociate atmospheric or ionospheric constituents. The TIEGCM uses a heating efficiency to parameterize the heating due to the solar EUV radiation, defined as the ratio of the heat directly deposited via fast atomic processes to the solar energy input at a given location. This is a simplified approach to estimating the neutral gas heating resulting from absorption of solar radiation. Since the EUV fluxes themselves are uncertain, variations of at least 10–20% in the heating efficiency are not unreasonable.

Better knowledge of the electron densities, particularly at night and at low altitudes, are necessary to make progress in understanding low-latitude electrodynamics, especially for the ion drifts. Since the neutral and ionized atmospheres are tightly coupled at low latitudes, simultaneous measurements of the neutral winds would be extremely useful in the electrodynamics investigations. Since the high altitude flux of O^+ is a major unknown which has significant impact on the model simulations, detailed knowledge of the fluxes, including the seasonal and solar cycle variation, would be valuable.

Several years ago, Anderson et al. (1998) reported the results of a project to simulate the middle-latitude ionosphere. The models CTIM, TIEGCM, and FLIP, along with the global time-dependent F region model based on that of Anderson (1973) and the Utah State University time-dependent ionosphere model (e.g., Schunk, 1988) were challenged to predict n_{max} and h_{max} observations from Millstone Hill during winter and summer for solar cycle minimum and maximum. As part of the ensuing collaboration, the modelers strove to ensure that the models were consistent; i.e., that each model used the same parameterizations, reaction rates, O^+–O collision frequency, diffusion rates, etc. A similar effort focused on low latitudes promises to be both illuminating and productive.

Acknowledgements

This work was supported by NSF Grants ATM 9796035 and ATM 9813863 to CGF; BWR was supported by AFRL contract F19628-96-C-0159. Boston University scientists acknowledge support from the NSF CEDAR program for the MISETA consortium. The Jicamarca Radio Observatory is operated by the Geophysical Institute of Perú, Ministry of Education, with support from the NSF cooperative agreements ATM-9022717 and ATM-9408441 to Cornell University. The National Center for Atmospheric Research provided computing time and assistance; NCAR is sponsored by the National Science Foundation.

References

Abdu, M.A., Reddy, B.M., Walker, G.O., Hanbaba, R., Sobral, J.H.A., Fejer, B.G., Woodman, R.F., Schunk, R.W., Szuszczewicz, E.P., 1998. Processes in the quiet and disturbed equatorial-low-latitude ionosphere: SUNDIAL campaign 1984. Annales de Geophysique 6, 69–80.

Anderson, D.N., 1973. A theoretical study of the ionospheric F region equatorial anomaly: 2. Results in the American and Asian sectors. Planetary and Space Science 21, 421–442.

Anderson, D.N., Buonsanto, M.J., Codrescu, M., Decker, D., Fesen, C.G., Fuller-Rowell, T.J., Reinisch, B.W., Richards, P.G., Roble, R.G., Schunk, R.W., Sojka, J.J., 1998. Intercomparison of physical models and observations of the ionosphere. Journal of Geophysical Research 103, 2179–2192.

Banks, P., 1966. Collision frequencies and energy transfer: ions. Planetary and Space Science 14, 1105–1122.

Bilitza, D., 1986. International reference ionosphere: recent developments. Radio Science 21, 343–346.

Biondi, M.A., Sazykin, S.Y., Fejer, B.G., Meriwether, J.W., Fesen, C.G., 1999. Equatorial and low-latitude thermospheric winds: measured quiet time variations with season and solar flux from 1980 to 1990. Journal of Geophysical Research 104, 17,091–17,106.

Buonsanto, M.J., Sipler, D.P., Davenport, G.B., Holt, J.M., 1997. Estimation of the O^+, O collision frequency from coincident radar and Fabry–Perot observations at Millstone Hill. Journal of Geophysical Research 102, 17,267–17,274.

Burnside, R.G., Tepley, C.A., Wickwar, V.B., 1987. The O^+–O collision cross-section: can it be inferred from aeronomical measurements? Annales de Geophysique Series A 5, 343–350.

Burnside, R.G., Sulzer, M.P., Walker, J.C.G., 1988. Determination of thermospheric temperatures and neutral densities at Arecibo from the ion energy balance. Journal of Geophysical Research 93, 8642–8650.

Burnside, R.G., Tepley, C.A., Sulzer, M.P., 1991. World Day observations at Arecibo: 1985–1989. Journal of Geophysical Research 96, 3691–3710.

Codrescu, M.V., Fuller-Rowell, T.J., Foster, J.C., 1995. On the importance of *E*-field variability for Joule heating in the high-latitude thermosphere. Geophysical Research Letters 22, 2393–2396.

Dickinson, R.E., Ridley, E.C., Roble, R.G., 1975. Meridional circulation of the thermosphere: 1. Equinox conditions. Journal of Atmospheric Science 32, 1737–1754.

Evans, J.V., 1975. A study of F2 region nighttime vertical ionization fluxes at Millstone Hill. Planetary and Space Science 23, 1611–1623.

Farley, D.T., 1991. Early incoherent scatter observations at Jicamarca. Journal of Atmospheric and Solar-Terrestrial Physics 53, 665–676.

Fejer, B.G., de Paula, E.R., Gonzalez, S.A., Woodman, R.F., 1991. Average vertical and zonal F region plasma drifts over Jicamarca. Journal of Geophysical Research 96, 13,901–13,906.

Fesen, C.G., 1997. Theoretical effects of tides and geomagnetic activity on the low latitude ionosphere. Journal of Atmospheric and Solar-Terrestrial Physics 59, 1521–1531.

Fesen, C.G., Roble, R.G., Ridley, E.C., 1991. Thermospheric tides at equinox: simulations with coupled composition and auroral forcings: 2. Semidiurnal component. Journal of Geophysical Research 96, 3663–3677.

Fesen, C.G., Roble, R.G., Richmond, A.D., Crowley, G., Fejer, B.G., 2000. Simulation of the pre-reversal enhancement in the low-latitude vertical ion drifts. Geophysical Research Letters 27, 1851–1854.

Forbes, J.M., Vial, F., 1989. Monthly simulations of the solar semidiurnal tide in the mesosphere and lower thermosphere. Journal of Atmospheric and Solar-Terrestrial Physics 51, 649–661.

Forbes, J.M., Roble, R.G., Fesen, C.G., 1993. Acceleration, heating, and compositional mixing of the thermosphere due to upward propagating tides. Journal of Geophysical Research 98, 311–321.

Fuller-Rowell, T.J., Codrescu, M.V., Moffett, R.J., Quegan, S., 1996. On the seasonal response of the thermosphere and ionosphere to geomagnetic storms. Journal of Geophysical Research 101, 2343–2353.

Hedin, A.E., 1991. Extension of the MSIS thermosphere model into the middle and lower atmosphere. Journal of Geophysical Research 96, 1159–1172.

Hernandez, G., Roble, R.G., 1977. Direct measurements of nighttime thermospheric winds and temperatures: 3. Monthly variations during solar minimum. Journal of Geophysical Research 82, 550–551.

McLandress, C., Shepherd, G.G., Solheim, B.H., Burrage, M.D., Hays, P.B., Skinner, W.R., 1996. Combined mesosphere/thermosphere winds using WINDII and HRDI data from the upper atmosphere research satellite. Journal of Geophysical Research 101, 10,441–10,453.

Mendillo, M., Baumgardner, J., Colerico, M., Nottingham, D., 1997. Imaging science contributions to equatorial aeronomy: initial results from the MISETA program. Journal of Atmospheric and Solar-Terrestrial Physics 59, 1587–1599.

Millward, G.H., Moffett, R.J., Quegan, S., Fuller-Rowell, T.J., 1996. A coupled thermosphere ionosphere plasmasphere model (CTIP). In: Schunk, R.W. (Ed.), Handbook of Ionospheric Models, STEP Report, Utah State University.

Oliver, W.L., Glotfelty, K., 1996. O^+–O collision cross section and long-term F region O density variations deduced from the ionospheric energy budget. Journal of Geophysical Research 101, 21,769–21,784.

Park, C.G., Banks, P.M., 1974. Influence of thermal plasma flow on the mid-latitude nighttime F_2 layer: effects of electric fields and neutral winds inside the plasmasphere. Journal of Geophysical Research 79, 4661–4668.

Pesnell, W.D., 1993. Momentum transfer collision frequency of O^+–O. Geophysical Research Letters 20, 1343–1346.

Reinisch, B.W., Huang, X., 1999. Low-latitude digisonde measurements and comparisons with IRI. Advances in Space Research 18, 6–12.

Richards, P.G., Torr, D.G., 1988. Ratio of photoelectron to EUV ionization rates for aeronomic studies. Journal of Geophysical Research 93, 4060–4066.

Richmond, A.D., Ridley, E.C., Roble, R.G., 1992. A thermosphere/ionosphere general circulation model with coupled electrodynamics. Geophysical Research Letters 19, 601–604.

Salah, J.E., Johnson, R.M., Tepley, C.A., 1991. Coordinated incoherent scatter radar observations of the semidiurnal tide in the lower thermosphere. Journal of Geophysical Research 96, 1071–1081.

Schmidtke, Doll, G.H., Wita, C., 1993. The variation of solar EUV/UV radiation of the steeply rising solar cycle 22 during the San Marco-5 Mission. Advances in Space Research 13 (1), 221–246.

Schunk, R.W., 1988. A mathematical model of the middle and high-latitude ionosphere. Pure and Applied Geophysics 127, 255–303.

Sica, R.J., Schunk, R.W., Wilkinson, P.J., 1990. A study of the undisturbed mid-latitude ionosphere using simultaneous multiple site ionosonde measurements during the SUNDIAL-86 campaign. Journal of Geophysical Research 95, 8271–8279.

Sulzer, M.P., Gonzalez, S.A., 1999. The effect of electron coulomb collisions on the incoherent scatter spectrum in the F region at Jicamarca. Journal of Geophysical Research 104, 22,535–22,551.

Szuszczewicz, E.P., Fejer, B., Roelof, E., Schunk, R., Wolf, R., Leitinger, R., Abdu, M., Reddy, B.M., Joselyn, J., Wilkinson, P., Woodman, R., 1988. SUNDIAL: a world-wide study of interactive ionospheric processes and their roles in the transfer of energy and mass in the Sun–Earth system. Annales de Geophysique 6, 3–18.

Szuszczewicz, E.P., Wilkinson, P., Abdu, M.A., Roelof, E., Hanbaba, R., Sands, M., Kikuchi, T., Burnside, R., Joselyn, J., Lester, M., Leitinger, R., Walker, G.O., Reddy, B.M., Sobral, J., 1990. Solar–terrestrial conditions during SUNDIAL-86 and empirical modeling of the global-scale ionospheric response. Annales de Geophysique 8, 387–398.

Szuszczewicz, E.P., Torr, D., Wilkinson, P., Richards, P., Roble, R., Emery, B., Lu, G., Abdu, M., Evans, D., Hanbaba, R., Igarashi, K., Jiao, P., Lester, M., Pulinets, S., Reddy, B.M., Blanchard, P., Miller, K., Joselyn, J., 1996. F region climatology during the SUNDIAL/ATLAS I campaign of March 1992: model-measurement comparisons and cause–effect relationships. Journal of Geophysical Research 101, 26,741–26,758.